South African Journal of Geomatics, Vol. 10. No. 1, February 2021

Regional ionospheric total electron content over Africa from ground-based GNSS observations

M. Moses[1], J. D. Dodo[2], L. M. Ojigi[1], K. Lawal[1]

[1] Department of Geomatics, Ahmadu Bello University, Zaria, Kaduna, Nigeria
[2] Centre for Geodesy and Geodynamics, NASRDA, Toro, Bauchi State, Nigeria
mosesmefe@gmail.com

DOI: http://dx.doi.org/10.4314/sajg.v10i1.2

Abstract

Due to the wide use of GNSS receivers both on satellites at low earth orbit and on the ground, continuous and long-time ionospheric data with increasing accuracy have been obtained and used to study variations in the Earth's ionosphere. Daily data from 2010.001 to 2017.365 sampled at 30 seconds from 104 African Geodetic Reference Frame (AFREF) dual-frequency GNSS Continuously Operating Reference Stations receivers distributed across Africa, were used in this study. Single Layer Model which assumes that all free electrons are concentrated in a shell of infinitesimal thickness, provides determining ionospheric total electron content value. In this study, the SLM model was used to derive total electron content values. TEC values obtained from the AFREF GNSS CORS measurements were compared with the TEC values from the global ionosphere maps provided by the Centre for Orbit Determination in Europe (CODE). The comparison was achieved by means of time series and wavelet analyses, and also by considering various model validation metrics. Comparative results for TEC estimates from both datasets based on goodness of fit measures, time series and wavelet analyses show good agreement on a statistical basis (r = 0.948) within the limits of experimental observation.

Keywords: *AFREF, GIM, Total Electron Content, wavelet*

1. Introduction

The ionosphere is around 60–1000 km over the earth's surface; it is a plasma of gas in the upper air ionized by sunlight based radiation and high energetic particles from the Sun. The ionized electron concentration vary with height above the earth's surface, position, time, season, and the measure of solar events. Ionosphere is also the main area of human's space activities. The extreme unsettling influence and transportation of energy and mass, which happens in the ionosphere, can impact space vehicles and their communication with stations on Earth. So ionospheric space weather has vital influence in human's economy and even day by day life (Alcay *et al.,* 2012; Panda *et al.,* 2020).

The International GNSS Service (IGS) of the International Association for Geodesy (IAG) maintains a global GNSS tracking network of GNSS receivers. The availability of a huge number of the IGS ground-based permanent dual frequency GNSS receivers, which are distributed over the Earth's surface, presents a tool for monitoring global patterns of ionospheric space weather. As a result of the wide use of GNSS receivers both on satellites at low earth orbit and on the ground in recent times, continuous and long-time ionospheric space weather data with increasing accuracy have been obtained and used to analyse the diurnal, seasonal and solar cycle variations of the ionospheric parameters over the Earth (Stolle *et al.*, 2013; Ren *et al.*, 2016; Moses et al., 2020).

Africa has the most tropical landmass area in the world (Eze, 2008). In fact, there is more danger of satellite signals or communication navigation systems being disrupted at tropical latitudes than elsewhere (Kintner *et al.*, 2009). In addition, Africa has the largest landmass beneath the geomagnetic equator and it serves as a natural platform to study ionospheric disturbances that affect navigation and communication systems (Amory-Mazaudier *et al.*, 2005; Yizengaw *et al.,* 2011). Therefore, understanding the physics behind the equatorial ionospheric irregularities is becoming critical to our daily life. Appropriate monitoring and forecasting of space weather is essential for the general public which depends increasingly on advanced technology that depends on continuous power accessibility, radio wave communication, navigation, and satellite operation. Aviation industry equipment can likewise be affected by ionospheric energetic particles. Ionospheric disturbances can interfere with aircraft communications predominantly at high-altitude and high-latitude flights. Despite the Earth's atmosphere offering some protection, unexpected solar events may still cause damages.

Furthermore, ionospheric delay is considered one of the prevalent error sources in GNSS. Without detecting the ionospheric delays resulting from ionospheric scintillation or disturbances, GNSS users could be placed under numerous dangerous circumstances. Users lacking ionospheric prediction and forecast information may be badly affected when a total or partial loss of communication occurs due to dramatic variations in the ionosphere (Choi *et al.*, 2012).

Considering potential space weather threats, reliable and permanent ionosphere monitoring and prediction is required to notify users in time on potential ionospheric threats during ionospheric storms and scintillations (Jakowski *et al.*, 2012; Zakharenkova *et al.*, 2012; Ahmed *et al.*, 2016). Monitoring the state of the ionosphere and long-term prediction serve an important objective in frequency planning and management procedures, and hence, comprehensive information on ionospheric activities has been among the most significant concerns in safety-critical timing applications and positioning (Choi *et al.*, 2012).

Observations of the African ionospheric space weather are currently limited due to lack of suitable ground-based space physics instrumentation (radars, magnetometers, ionosondes, etc.) (Yizengaw, 2012). Therefore, there has been less extent of the spatial and temporal imaging of the African ionosphere and related phenomena, with previous studies carried out over short periods at specific stations or sub-

regions see (Opperman, 2007; Moeketsi *et al.*, 2007; Habarulema, McKinnell and Opperman, 2010; Adewale *et al.*, 2011; Ouattara and Fleury, 2011; Olwendo *et al.*, 2012; Christian *et al.*, 2012; Fayose *et al.*, 2012; Habarulema and Mckinnell, 2012; Oron, D'ujanga and Ssenyonga, 2013; Christian, Frederic and Francois, 2013; Oryema *et al.*, 2015; Oryema, Jurua and Ssebiyonga, 2016; Okoh *et al.*, 2016; Abe *et al.*, 2017; Moses, Dodo and Ojigi, 2018). Small-to-medium scale ionospheric variations and irregularities at low/mid-latitudes in the African region have not been studied in detail due to limited instrumentation. This has created a gap in the global understanding of the African ionosphere, which in turn, imposes severe limitations on ionospheric space weather monitoring efforts in the region. Coordinated ground- and space-based observations are therefore needed to unravel the knowledge of the African ionospheric space weather to provide a better understanding of its dynamics and variation in time and space and response to solar activity.

The manuscript is organized into four sections: (1) Introduction presenting the background to the study. (2) Methodology, where the data sources and regional TEC computation method are described (3) Results and Discussion where we present our study results and their discussions. Then, Section 4 presents the conclusions of TEC computation over the African region.

2. Methodology

In this study, data from over 100 continuously operating reference stations (CORS) within Africa located between latitudes ±40º longitudes -20º W to 55º E were used in estimating the regional ionospheric TEC over Africa. Daily RINEX data at the respective stations from 2010 to 2017 were acquired. The spatial distribution of the AFREF and IGS stations used, ionosondes stations as well as the Global Ionospheric Maps (GIM) grids over Africa are shown in the Figure 1.

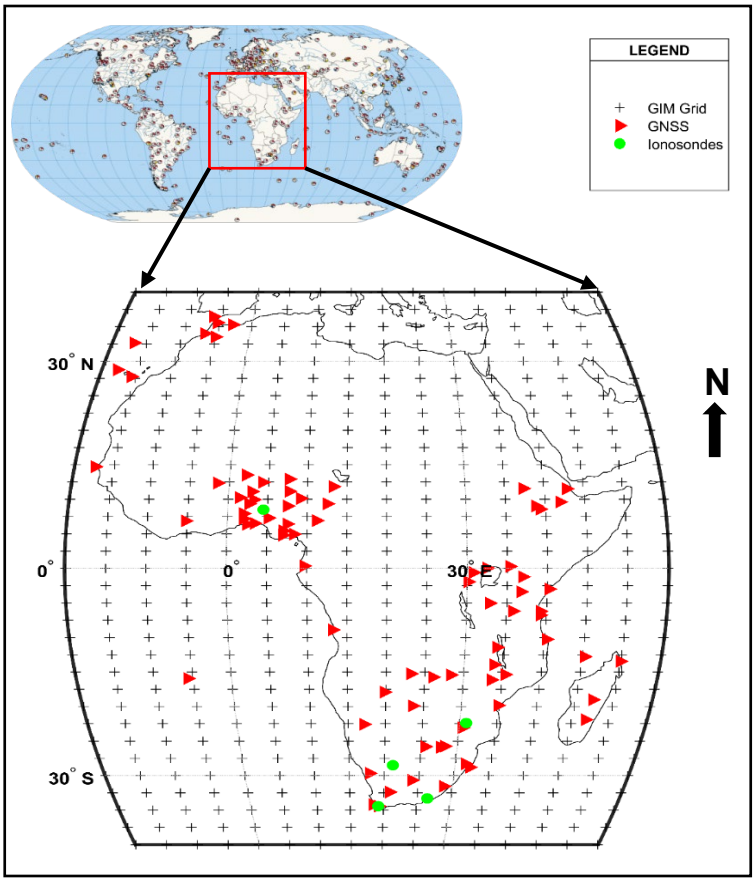

Figure 1: Map of study area with GNSS and Ionosondes stations

2.1. Ionospheric total electron content from Ground-based observations

The observation equations of ionospheric delay are expressed as follows:

$$P_i = \rho - \frac{40.3}{f_i^2} F(z) \times TEC + b^s - b^r + \Delta \ , \quad i = 1,\ 2 \tag{1}$$

$$\Phi_i \lambda_i = \rho - \frac{40.3}{f_i^2} F(z) \times TEC - N_i \lambda_i + B^s - B^r + \Delta \ , \quad i = 1,\ 2 \tag{2}$$

(Ya'acod *et al.,* 2010; Krypiak-Gregorczyk, and Wielgosz, 2018)

Where i is the number of signal frequency, P is the pseudorange, ϕ is the carrier phase, ρ is the geometric distance from the receiver to the satellite, f is the frequency, $F(z)$ is the mapping function with respect to the elevation angle z, b^s is the satellite circuit delay error of pseudorange, b^r is the receiver circuit delay error of pseudorange, B^s is the satellite circuit delay error of phase, B^r is the receiver circuit delay error of phase, λ is the wave length, N is the integer ambiguity, and Δ is the correction term including receiver clock error, satellite clock error, troposphere delay, multipath correction. TEC can then be calculated according to the pseudorange and phase data in the following way:

$$TEC = -\frac{1}{40.3F(z)}\frac{f_1^2 f_2^2}{f_1^2 - f_2^2}\left(P_4 - dcb\right) \quad (3)$$

$$TEC = -\frac{1}{40.3F(z)}\frac{f_1^2 f_2^2}{f_1^2 - f_2^2}\left(L_4 - \Delta Amb - DCB\right) \quad (4)$$

Where:

$P_4 = P_1 - P_2$,

$L_4 = \phi_1\lambda_1 - \phi_2\lambda_2$,

$dcb = (b_1^s - b_2^s) - (b_1^r - b_2^r)$,

$DCB = (B_1^s - B_2^s) - (B_1^r - B_2^r)$,

$\Delta Amb = N_2\lambda_2 - N_1\lambda_1$.

The processing was carried out by means of the GPS TEC analysis application provided by the Institute for Scientific Research, Boston College, Boston, MA, USA (Gopi, 2014) using data sampled at 30 seconds from the daily GNSS ground-based observations of all operational AFREF CORS distributed within Africa. The software calculates the slant TEC (STEC) from the 30 seconds observation data and the STEC values are converted to vertical TEC (VTEC) values by means of a suitable mapping function.

The mapping function $F(z)$ is given by:

$$F(z) = \frac{1}{\sqrt{1 - \left(\frac{R_e}{R_e + h_i}\cos(r_e)\right)^2}} \quad (5)$$

Where R_e is the radius of the earth (~6371km); h_i is the effective height of the single-layer model; r_e is the elevation at a receiver station.

(Ya'acod *et al.,* 2010; Krypiak-Gregorczyk, and Wielgosz, 2018)

The final VTEC values are provided with one-minute intervals. The ionospheric dataset used for the purpose of comparison it the Global Ionospheric Maps, are provided by the Centre for Orbit Determination in Europe located at the University of Berne, Switzerland via file transfer protocol (ftp://ftp.unibe.ch/aiub). The spatial resolution of these maps is 2.5 degree in latitude and 5 degree in longitude, and their time resolution is 2 hours. Each daily file includes 13 ionosphere maps, starting from 0:00 to 24:00 hours, thus each map covers a 2 hours period. TECs of global grids are reconstructed by fitting the vertical TECs of IGS stations with the spherical harmonics function.

$$TEC(\alpha,\beta) = \sum_{n=0}^{n_{\max}}\sum_{m=0}^{n} P_{nm}\sin(\alpha)\left[a_{nm}\cos(m\beta) + b_{nm}\sin(m\beta)\right] \quad (6)$$

Where α and β are the latitude and longitude respectively, n is the highest degree, $P(\alpha)$ is the normalised associated Legendre function, a and b are the spherical harmonics coefficients, and n and m are degree and order, respectively (Guo *et al.*, 2017). Figure 2 shows the flowchart for GNSS ground-based ionospheric TEC retrieval system over Africa.

2.2. Retrieval of ionospheric parameters from AFREF and IGS ground networks

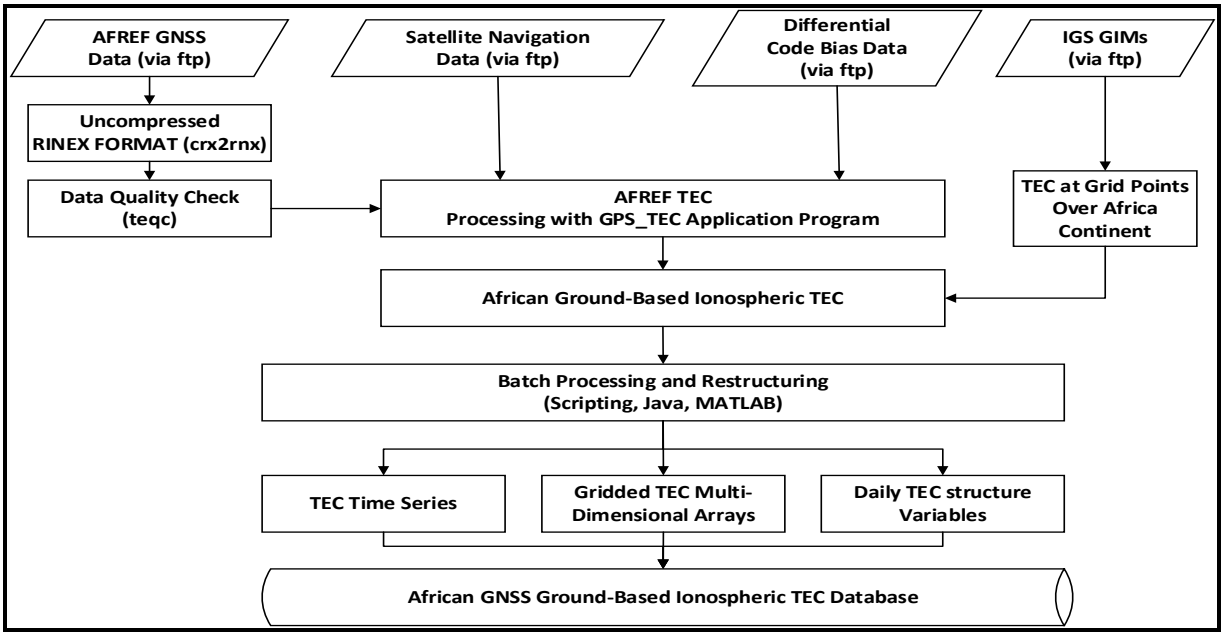

Figure 2: Flowchart for GNSS ground-based ionospheric TEC retrieval system over Africa

Archived daily 30s epochs GNSS observation data in compact RINEX format from operational AFREF CORS from 2010-2017 were filed via file transfer protocol (ftp) from the AFREF server (freely available at ftp://afrefdata.org) by means of the Filezilla application and custom batch scripts implementation of wget application . The observation files were then un-compressed using crx2rnx Hatanaka to RINEX conversion program which converts the observation data from ".D" extension to ".O" ready for post-processing. Satellite navigation data from website (ftp://cddis.gsfc.nasa.gov/pub/gps/data/daily) and Differential Code Biases (DCBs) data for Satellites and Receivers from the University of Berne, Switzerland, were also filed via custom batch automatic ftp scripts.

The AFREF GNSS RINEX data editing and validation process was performed using a quality check program UNAVCO's teqc program which was obtained from the IGS Central Bureau Information System. The data are validated and edited for quality control by checking:

i. the header-file information (station name, receiver/antenna information, antenna height);
ii. the number of GPS observations (completeness of data);
iii. the number of observed satellites;
iv. the date and times of first and last observation record.

The ground-based ionospheric parameter retrieval for the AFREF stations was carried out using the resulting RINEX files, satellite navigation data and the Differential Code Bias files for each day by means of the GPS TEC processing application (Gopi, 2014) at one minute temporal resolution.

The slant (STEC) calculated from phase and group TEC which is polluted with the receiver and satellite biases. Hence, desired

$$\text{slant TEC} = \text{STEC} + \text{BRx} + \text{BRich} + \text{Bsat} \quad (7)$$

Where BRx, BRich, Bsat are receiver bias, receiver inter-channel bias and satellite biases respectively (Gopi, 2014). A total of 122,451 daily GNSS observation data from the AFREF CORS from 2010 to 2017 were processed in order to retrieve ionospheric TEC values from GNSS ground-based observations over Africa.

GIMs are representative of the TEC values at grid points over the globe determined from GNSS observations. They are obtained from GPS/GLONASS data mainly from the IGS stations. The spatial resolution of these maps is 2.5 degree in latitude and 5 degree in longitude, and their time resolution is 2 hours. Each daily file includes 13 ionosphere maps, starting from 0:00 to 24:00 hours, thus each map covers a 2 hours period (Guo *et al.,* 2017). Extraction of vertical total electron content (VTEC) at grid pints covering Africa from the Global Ionospheric Maps (GIMs) and archiving as multi-dimensional array for easy retrieval and further analysis was carried out processing daily data from years 2010-2017 with 13 maps per day at 2 hours temporal resolution and a spatial resolution of 2.5◦ x 5◦ in latitude and longitude respectively. A total of **42,731** GIMs were processed to retrieve ionospheric TEC values over the entire African continent.

Custom computer programs written in batch scripting, Java and MATLAB high level programming languages were implemented for the batch processing and archiving of the GPS TEC processing application and GIMs outputs into TEC time series, daily structured TEC variables and multi-dimensional arrays resulting to a robust regional ionospheric TEC database for Africa.

3. Results and Discussion

3.1. African regional ionospheric TEC from AFREF GNSS and GIMs observations

The ground-based ionospheric TEC have been derived from processing the daily GNSS data from all operational AFREF CORS, and also from the Global Ionospheric Maps provided by IGS for comparison. The comparison of the ground-based ionospheric datasets was achieved by analysing the time series, wavelet power spectrum and goodness of fit measures using results for periods common to both datasets. Figure 3 shows the comparison of AFREF and GIM derived ionospheric TECs over Africa.

Figure 3a shows eight years mean diurnal TEC time series derived from the AFREF network and from IGS GIMs. The AFREF derived TEC has been shown by continuous red line while the GIMs derived

TEC has been represented by continuous solid blue line. Figure 3b shows the comparative plot and correlation results of both datasets to provide an indication of the reliability of the AFREF results, while Figure 3c and Figure 3d show the wavelet power spectra for the AFREF and GIM derived ionospheric TEC respectively, in order to analyse the temporal evolution of the frequency content of both TEC time series. Figure 4 presents the goodness of fit measures between the AFREF and GIM TECs.

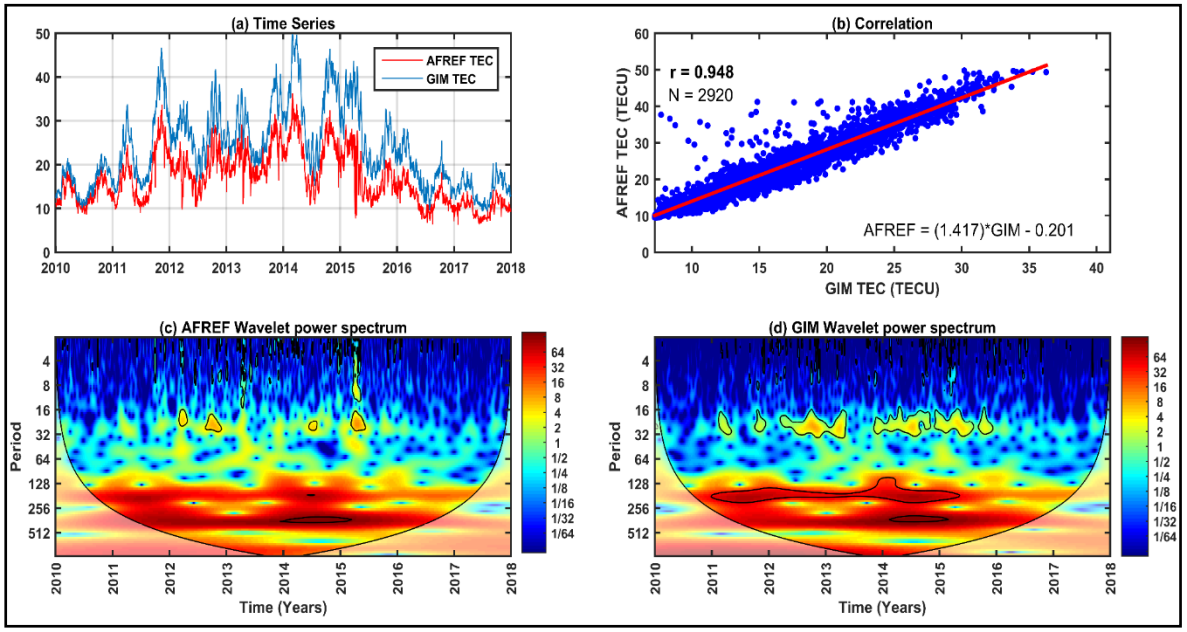

Figure 3: Comparison of AFREF and GIM derived ionospheric TECs over Africa. (a) Eight years diurnal TEC time series (b) Correlation coefficient computed by fitting a linear regression between AFREF and GIM TEC over Africa, (c) wavelet power spectrum of the AFREF TEC, (d) wavelet power spectrum of the GIM TEC

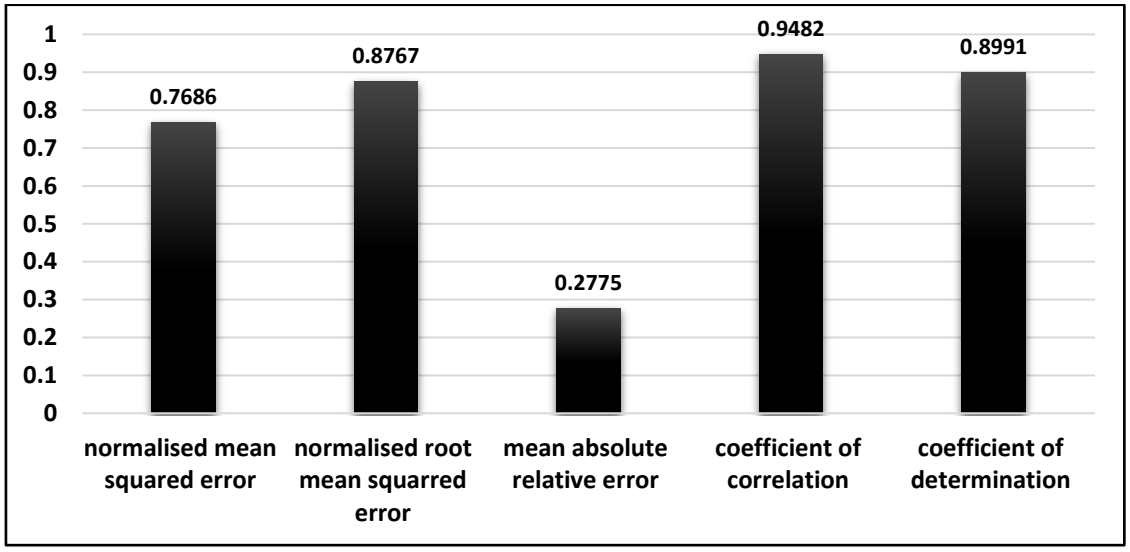

Figure 4: Goodness of fit measures between AFREF and GIM TECs

The comparative plots and goodness of fit measures show good statistical agreement between the two datasets. There is a very good correlation ($r = 0.9482$; $r^2 = 0.8991$) between the two TEC datasets over the African region as shown in Figure 3(b). Thus, over 94% variation in the AFREF derived TEC is explained by the GIM TEC. Moreover, TECs computed from both models depict low power spectra in the beginning periods between 1 and 16. Also, both datasets exhibit daily peaks, annual and semi-annual periodicities, and having very similar wavelet power spectra (Figure 3(c) and (d)). The goodness of fit measures are computed to see how effectively the AFREF and GIM TECs estimates the behaviour of the ionosphere over Africa. The normalised mean squared error, normalised root mean squared error and mean absolute relative error shown in Figure 4 are well below 1TECU, indicating less residual variance between both dataset, although there is a minor increase in the absolute values of TEC for the GIM estimation compared to those for the AFREF values.

For the purpose of explanatory data analysis, the boxplot in Figure 5 visually displays the data distribution of the two TEC datasets based on the five number summary: minimum, first quartile, median, third quartile, and maximum. The graph shows the shape of the distributions, their central value and variability for the period of year 2010 to 2017. The ends of the box are the upper and lower quartiles, thus, the box spans the interquartile range. The median is marked by a circle with black dot at the centre inside the box. Additionally, the annual mean TEC for each year is indicated by the solid red lines in both distributions.

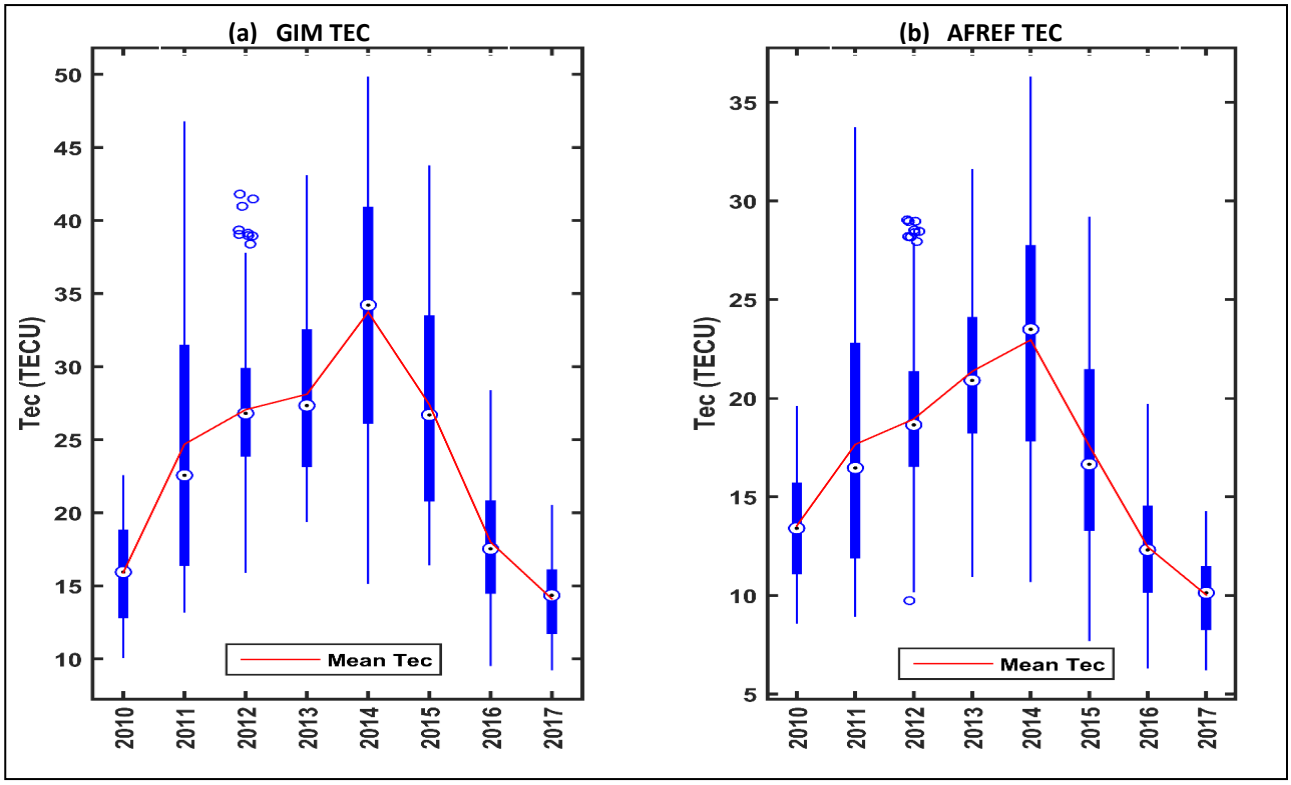

Figure 5: Summary statistics of AFREF and GIM TECs over Africa

It can be observed from the summary statistics shown in Figure 5 that the AFREF and GIM derived TECs follow similar annual trend, with the GIM TEC having a slightly steeper increase in TEC between year 2013 and 2014 as compared to the gentle increment recorded by the AFREF datasets. Also, both datasets only recorded some outlier values only in the year 2012. As represented by the boxplots, the GIM model five number summary tend to have higher values that the corresponding AFREF five number summary. This can be attributed to the historically lack of sufficient IGS CORS data coverage within the African continent leading to generalisation of the TEC over Africa by the GIM.

3.2. Wavelet analysis of GIM and AFREF TEC time series

In order to further reveal localized similarities in time and scale of the two ionospheric TECs over the African continent, cross examination of the two TEC decompositions from the AFREF and IGS GIMs was carried out by means of wavelet analysis. Figure 6 shows the cross wavelet power spectrum and wavelet coherence spectrum between the GIM and AFREF TECs. The arrows in Figures 6a and 6b signify the relative phase between the two TEC signals as a function of scale and position derived from the smoothed estimate of the wavelet cross spectrum. The plot of the relative phases was also superimposed on the wavelet coherence. The relative phase information produces a local measure of the delay between the two TEC time series.

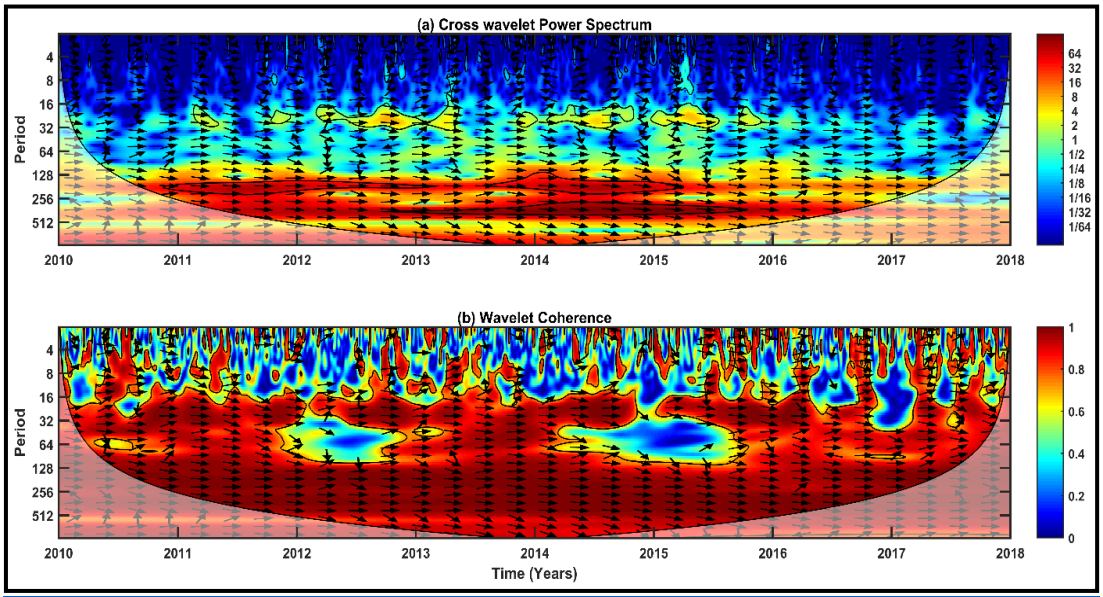

Figure 6: Wavelet analysis of GIM and AFREF TEC time series from 2010to 2017 a) is the cross wavelet power spectrum b) wavelet coherence spectrum.

In Figure 6, the right arrow represents the same phase, the down arrow represents the phase leading 90 degrees, left arrow represents the antiphase, and the up arrow represents the phase leading 270 degrees. The numerical value of the local covariance between the time series in the time-scale plane is interpreted as the magnitude of the wavelet cross spectrum indicate a signals. A relationship between the

signals is indicated by regions in the time and frequency plane where the two time series exhibit common power or consistent phase characteristics. The magnitude is the more instructive and shows the similarity of the local frequency behaviour of the two TEC time series in the time-scale plane.

Both signals have a similar contribution around scale greater than 128 over the entire time interval. This is consistent with the behaviour observed by visual inspection of the time-domain plot. The modulus of the wavelet cross spectrum clearly shows a strong component for most of the periods. The magnitude of the component increases and decreases over time, but is generally stronger for periods greater than approximately 128 of the signals.

Additional remarkable information is noticeable in the wavelet coherence analysis of the two TEC time series (Figure 6(b)). The phase information can be interpreted by pinpointing different regions of the time-scale plane and underlining some coherent behaviours. Some transient minor contributions to the variability of the time series occur at small scales (1-16) at the beginning of the TEC signal, which exhibits rapid oscillations. The behaviour is not very coherent during these period, and the phase changes very quickly. However, and scale periods greater than 16 at all positions in the time domain (2010 to 2017), numerous coherent regions with coherence of or near one can be easily detected, delimited by the stability of the phase information (direction of the arrows). Because phase information is so useful in determining coherent behaviour, another representation tool is available for focusing on the phase. The arrow and vector orientation is use to code the phase information. Finally, computing the wavelet coherence and superimposing the phase of the smoothed wavelet cross spectrum shows that TEC data from the two datasets exhibit coherence near one (1) and approximately constant relative phase at the various scales, as there rarely exist any noticeable anti-phases between the two TEC time series.

From the time series analysis, goodness of fit measures, and the wavelet power spectrum analysis, it has been established that performance of the AFREF and GIM derived TEC datasets are comparable both in time and space. The cross wavelet and wavelet coherence analyses further establish the fact that both datasets are highly coherent and in phase for most of the periods. It is concluded that the TEC estimates from the two independent techniques agree well on a statistical basis within the limits of experimental observation. Therefore, the consistent and readily available GIMs serve as very adequate datasets to be used as reference for time periods where continuous AFREF derived TEC are not readily available possibly due to technical and/or power problems.

4. Conclusions

The existing global ionospheric models such as CODE GIMs although able to account for most of the ionospheric variations within the African region, they still have low spatio-temporal resolution. In this paper, a regional ionospheric TEC estimation over Africa from over 100 continuously operating ground-based GNSS stations within the region has been carried out with a one minute resolution. The ground-

based datasets of AFREF and GIM TECs adequately model the African ionospheric space with very strong positive correlation and fascinating similitude in their wavelet power spectra. Our results show that the TEC measurements from the two independent techniques agree well on a statistical basis within the limits of experimental observation. Thus, GIM-derived TEC values can be used for the locations where continuous AFREF TEC data are not available.

Conflicts of Interest: The authors declare no conflict of interest.

5. References

Abe, O. E., Villamide, X. O., Paparini, C., Radicella, S. M. and Nava, B. (2017) 'Analysis of a Grid Ionospheric Vertical Delay and Its Bounding Errors over West African Sub-Saharan Region', *Journal of Atmospheric and Solar-Terrestrial Physics*, 154, pp. 67–74.

Adewale, A. O., Oyeyemi, E. O., Adeloye, A. B., Ngwira, C. M. and Athieno, R. (2011) 'Analysis of a Grid Ionospheric Vertical Delay and Its Bounding Errors over West African Sub-Saharan Region', *Journal of Geophysical Research*, 116, p. A12319. doi: 10.1029/2011JA01699.

Ahmed, W. A., Agbaje, G. I., Ayeiola, S. Y., Balogun, B. O., Echoda, N. J. A., Onimago, Y, A. and Olunuga, T. (2016) 'Determination of Total Electron Content at Equatorial Region — Thailand Using Radio Occultation Technique', *Atmospheric and Climate Sciences*, 6, pp. 319–328. doi: 10.4236/acs.2016.62027.

Alcay, S., Inal, C., Yigit, C.O., and Yetkin, M. (2012) 'Comparing GLONASS only with GPS only and hybrid positioning in various length of baselines'', *Acta Geodaetica et Geophysica*, *47*(1), pp. 1-12. doi: 10.1556/AGeod.47.2012.1.1

Amory-Mazaudier, C., Kobea, A., Vila, P., Achy-Seka, A., Blanc, E., Boka, K. and Lathuillere, C. (2005) 'Equatorial Geophysics Studies: The IGRGEA Results During the Last Decade', *Journal of Atmospheric and Solar terrestrial Physics*, 67(4), pp. 301–313.

Ansari, K., Park, K.D. and Panda, S.K., (2019) 'Empirical orthogonal function analysis and modeling of ionospheric TEC over South Korean region', *Acta Astronautica*, 161, pp.313-324. DOI:10.1016/J.ACTAASTRO.2019.05.044

Choi, K. H., Kim, H. S., Lee, J. Y., Lim, J. H. and Lee, H. K. (2012) 'Real-time Monitoring of Detailed Regional Ionospheric Activities by GPS CORS Networks', in *The 14tth IAIN Congress 2012, Seamless Navigation (Challenges and Opportunities)*. Cairo, Egypt.

Christian, Z., Frederic, O. and Francois, Z. (2013) 'CODG tec variation during solar maximum and minimum over niamey', *European Scientific Journal*, 9(27), pp. 74–80.

Eze B.U. (2008) '*A Brief Outline on the Geographical Background of Africa*', In: Holbrook J.C., Urama J.O., Medupe R.T. (eds) African Cultural Astronomy. Astrophysics and Space Science Proceedings. Springer, Dordrecht. https://doi.org/10.1007/978-1-4020-6639-9_3

Fayose, R. S., Babatunde, R., Oladosu, O. and Groves, K. (2012) 'Variation of Total Electron Content [TEC] and their Effect on GNSS over Akure, Nigeria', *Applied Physics Research*, 4(2). doi: 10.5539/apr.v4n2p105.

Gopi, K. S. (2014) 'GPS-TEC analysis application'. Boston College, U.S.A: Institute for Scientific Research. Available at: http://seemala.blogspot.com/.

Guo, J., Dong, Z., Liu, Z., Mao, J. and Zhang, H. (2017) 'Study on ionosphere change over Shandong based from SDCORS in 2012', *Geodesy and Geodynamics*, 8(2017), pp. 229–237.

Habarulema, J. B. and Mckinnell, L. (2012) 'Investigating the performance of neural network backpropagation algorithms for TEC estimations using South African GPS data', *Annales Geophysicae*, 30(5), pp. 857–866. doi: 10.5194/angeo-30-857-2012.

Habarulema, J. B., McKinnell, L. A. and Opperman, B. D. (2010) 'TEC Measurements and Modelling over Southern Africa during Magnetic Storms; A Comparative Analysis', *Journal of Atmospheric and Solar Terrestrial Physics*, 72, pp. 509–520.

Jakowski, N., Beniguel, Y., De Franceschi, G., Pajares, M. H., Jacobsen, K. S., Stanislawska, I., Tomasik, L., Warnant, R. and Wautelet, G. (2012) 'Monitoring, tracking and forecasting ionospheric perturbations using GNSS techniques', *Journal of Space Weather and Space Climate*, 2012(2), p. A22.

Kintner, P. M., O'Hanlon, B., Gary, D. E. and Kintner, P. M. S. (2009) 'Global Positioning System and Solar Radio Burst Forensics', *Radio Science*, 44. doi: 10.1029/2008RS004039.

Krypiak-Gregorczyk, A., and Wielgosz, P. (2018) 'Carrier phase bias estimation of geometry-free linear combination of GNSS signals for ionospheric TEC modeling', *GPS Solutions, 22* **(**45). https://doi.org/10.1007/s10291-018-0711-4

Moeketsi, D. M., Combrinck, W. L., McKinnell, L. A. and Fedrizzi, M. (2007) 'Mapping GPS¬derived Ionospheric Total Electron Content over Southern Africa During Different Epochs of Solar Cycle 23', *Advances in Space Research*, 36, pp. 821–829.

Moses, M., Dodo, J. D. and Ojigi, L. M. (2018) 'Spatio-temporal and solar activity variation of ionospheric total electron content over the Nigerian GNSS CORS', *Nigerian Journal of Geodesy*, 2(1), pp. 109–134.

Okoh, D., Owolabi, O., Ekechukwu, C., Folarin, O., Arhiwo, G., Agbo, J. and Bolaji, S. (2016) 'A Regional GNSS-VTEC Model over Nigeria using Neural Networks : A Novel Approach', *Geodesy and Geodynamics*, 7(1), pp. 19–31. doi: 10.1016/j.geog.2016.03.003.

Olwendo, O. J., Baki, P., Cilliers, P. J., Mito, C. and Doherty, P. (2012) 'Comparison of GPS TEC measurements with IRI-2007 TEC prediction over the Kenyan region during the descending phase of solar cycle 23', *Advances in Space Research*, 49, pp. 914–921.

Opperman, B. D. L. (2007) *Reconstructing Ionospheric TEC over South Africa using Signals from a Regional GPS Network*. Rhodes University.

Oron, S., D'ujanga, F. M. and Ssenyonga, T. J. (2013) 'Ionospheric tec variations during the ascending solar activity phase at an equatorial station, Uganda', *Indian Journal of Radio and Space Physics*, 42(1).

Oryema, B., Jurua, E., D'Ujanga, F. M. and Ssebiyonga, N. (2015) 'Investigation of TEC variations over the magnetic equatorial and equatorial anomaly regions of the African sector', *Advances in Space Research*, 56(9). doi: 10.1016/j.asr.2015.05.037.

Oryema, B., Jurua, E. and Ssebiyonga, N. (2016) 'Variations of Crest-to-Trough TEC Ratio of the East African Equatorial Anomaly Region', *International Journal of Astrophysics and Space Science*, 4(1), pp. 12–20. doi: 10.11648/j.ijass.20160401.12.

Ouattara, F. and Fleury, R. (2011) 'Variability of CODG TEC and IRI 2001 Total Electron Content (TEC) During IHY Campaign Period (21 March to 16 April 2008) at Niamey under Different Geomagnetic Activity Conditions', *Scientific Research and Essays*, 6(17), pp. 3609–3622.

Panda, S.K., Reddybattula, K. D., Haralambous, H., and Sharma, S.K. (2020) 'Assessment of ionospheric variability fromIRI-2016, SPIM-2017, and IGS-GIM using Digisonde and GPS observations over Cyprus', *Astrophysics and Space Science* (2020) 365:37. https://doi.org/10.1007/s10509-020-03752-2

Stolle, C., Floberghagen, R., Luhr, H., Maus, S., Knudsen, D. J., Alken, P. and Visser, P. N. (2013) 'Space Weather Opportunities from the Swarm Mission including Near Real Time Applications', *Earth, Planets and Space*, 65, pp. 1375–1383. doi: 10.5047/eps.2013.10.002.

Ya'acob, N., Abdullah, M. E, and Ismail, M. (2010) 'GPS Total Electron Content (TEC) Prediction at Ionosphere Layer over the Equatorial Region', Trends in Telecommunications Technologies, Christos J Bouras (Ed.), ISBN: 978-953-307-072-8, InTech, DOI: 10.5772/8474. Retrieved from: http://www.intechopen.com/books/trends-in-telecommunications-technologies/gps-total-electro-content-tec-prediction-at-ionosphere-layer-over-the-equatorial-region.

Yizengaw, E. (2012) 'Ground-based Instrumentations in Africa and Its Scientific and Societal Benefits to the Region', in *39th COSPAR Scientific Assembly, PCB1-0008, 14-21 July 2012*. Mysore, India.

Zakharenkova, I. E., Krankowski, A., Shagimuratov, I. I., Cherniak, Y. V., Krypiak-Gregorczyk, A., Wielgosz, P. and Lagovsky, A. F. (2012) 'Observation of the ionospheric storm of October 11, 2008 using FORMOSAT-3/COSMIC data', *Earth, Planets and Space*, 64, pp. 505–512.